DEVELOPMENT OF THE UK NATIONAL ROTOR RIG FOR AEROELASTIC TESTING OF ROTARY WINGS

D. Zagaglia*, A.D. Croke, R.B Green, G.N. Barakos
James Watt School of Engineering, University of Glasgow
University Avenue, Glasgow, G12 8QQ, Scotland, UK
* Corresponding Author, e–mail: daniele.zagaglia@glasgow.ac.uk

Abstract
The development of a novel propeller rig for testing in stalled conditions is described in the present paper. The rig is the outcome of the recent adaptation of the ARA UK national rotor rig, undertaken at the University of Glasgow in the framework of the EPSRC funded MENtOR project. The rig allows for testing of a 1.25 m diameter propeller at tip Mach scaled conditions and pitch angles up to 40°. Blades are instrumented with seven full strain gauge bridges to monitor flap bending, lead-lag bending and torsion. Loads acting on the hub can be measured by means of a rotating shaft balance, and data is transferred from the rotating to the stationary frame of the rig by means of a telemetry system. This paper details the development, features and capabilities of the rig whilst also providing practical insight to considerations of integrating a complex rig into an existing wind tunnel. Sample results of a tiltrotor blade set at a stalled condition will be presented also.

Keywords: Wind Tunnel, Propeller, Stall, Strain Gauge, Aerodynamics, Aeroelastics.

NOMENCLATURE

Symbols

J	Advance ratio, $U_\infty/(nD)$, $(-)$
n	Propeller rotational frequency, (Hz)
R	Propeller radius, (m)
U_∞	Freestream velocity, (m/s)
x	Blade radial coordinate, (m)
$\beta_{0.75R}$	Blade pitch angle at 75% radius, $(^\circ)$
ΔP_{CON}	Pressure difference across WT contraction, (Pa)
ΔP_{PROBE}	Pressure difference at test section Pitot-Static probe, (Pa)
$\overline{\epsilon_B}$	Bridge compensated strain, $(-)$
ϵ_B	Bridge uncompensated strain, $(-)$
κ	Wind tunnel calibration constant, $(-)$
ρ	Air density, (kg/m^3)
Ω	Propeller rotational frequency, (RPM)

Acrynoms

ARA	Aircraft Research Association
CAA	Civil Aviation Authority
CFD	Computational Fluid Dynamics
CSD	Computational Structural Dynamics
CTA	Constant Temperature Anemometry
DIC	Digital Image Correlation
EASA	European Union Aviation Safety Agency
EPSRC	Engineering and Physical Sciences Research Council
eVTOL	Electric Vertical Take-off and Landing
FAA	Federal Aviation Administration
LDA	Laser Doppler Anemometry
MENtOR	Methods and Experiments for NOvel Rotorcraft
NACA	National Advisory Committee for Aeronautics
NASA	National Aeronautics and Space Administration
PIV	Particle Image Velocimetry
RPM	Revolutions Per Minute
RSB	Rotating Shaft Balance
UKNRR	United Kingdom National Rotor Rig
WT	Wind Tunnel

1. INTRODUCTION

The recent growth in the development of electrically driven aircraft has revitalised the requirement to further push the available testing capability of propellers and rotors. In order to certify future electric Vertical Take-off and Landing (eVTOL) designs, regulatory bodies such as EASA, CAA and FAA will require experimental data to satisfy the design and operational limits of these novel configurations. This has lead to a significant focus within the experimental community to develop state-of-the-art experimental setups that can be used to explore areas of interest such as propeller/rotor aeroelasticity and aerodynamics.

At present, experimental investigations into aeroelastic phenomenon such as rotary wing stall flutter have been severely restricted. This is a direct result of a clear lack of suitable testing infrastructure in addition to a very limited availability of facilities and personnel who can provide use of the precision instrumentation required to obtain meaningful results of these complex phenomena.

Experimental efforts to investigate blade flutter have taken place as early as the 1920's, making use of optical methods such as photosensitive paper to measure flutter amplitudes and frequencies from light reflected from the propeller blade [1]. In the 1930's, experimental campaigns to research rotary wing flutter flourished due to many unexplained propeller failures [2]. In 1935, Theodorsen [3] made use of a motion camera to capture bending and torsional deformations of rotating blades. Due to the restrictions of available camera technology, the experimental setup was limited by a lack of available light which was required to ensure sufficient image resolution at high rotational speeds.

Throughout the 1940's and 1950's, the wartime and and post war growth of commercial aviation resulted in a significant amount of aeroelastic testing of full-scale aircraft propellers in both static and forward advance conditions [4,5,6]. Generally, blades used during testing were manufactured from wood or metal alloys, due to the difficulties and cost of manufacturing complex shapes. Blades were also typically instrumented with both axial and shear strain gauges, where bridge readings were recorded using an oscillograph. As well as structural data, some investigations also logged flow data by making use of pressure probes located fore and aft of the propeller disk to measure propeller inflow and outflow. Wake rakes were also used to measure the momentum deficit in the wake, to provide an indication into the drag of the propeller. Load measurements were sparse, due to the complexity of integrating a Rotating Shaft Balance (RSB) to the propeller rig. Several works made use of single axis load cells to measure thrust and torque data.

Furthermore, in the late 1950's, ground testing and in-flight testing of thinner blade sections were also performed by NACA by mounting a series of propeller blade sets to the nose of a McDonnell XF-88B jet aircraft. This study focused on 1-P stresses that arise from oscillating aerodynamic loading, stall flutter blade characteristics and the effect of spinner shape on propeller inflow [7,8,9]. In-flight data was compared to earlier wind tunnel tests performed by Hubbard et al. [10].

Throughout the 1960's, the dawn of the jet age lead to a steep decline in propeller research. However, in the 1970's with soaring fuel costs [11] and the increasing dependency on the newly developed turbojet, NASA began to develop a high speed propeller with the hope of achieving higher propulsive efficiency. Between 1970 and 1990, NASA undertook a series of aeroelastic test campaigns of their high speed propeller concept, which utilised highly twisted and highly loaded SR-series blades. Areas of research included blade deformation, stall onset, dynamic response and blade mistuning [12,13,14,15]. Over 1000 hours of propeller aeroelastic testing concluded that classical flutter is understood sufficiently and propeller designs can be tuned during the design process [16]. Nonetheless, stall flutter remains a much more complex phenomena due to the aerodynamic non-linearity. Moreover, Dowty Rotol undertook a series of tests using blades instrumented with strain gauges for a range of rotational speeds and blade pitch settings [17]. Initial testing was terminated due to excessive noise signifying flutter.

Post the late 1980's, very little experimental work has been carried out on propeller stall flutter. The last significant propeller flutter investigation made publicly available was conducted by Podboy et al. [18] in 1993 at NASA, who made use of Laser Doppler Anemometry (LDA). Since then, many of the limited investigations have consisted of 2D flow around aerofoils undergoing pitch and heave motions at low Reynolds numbers [19,20,21]. Optical methods such as Particle Image Velocimetry (PIV) [21] have been used to study the flow topology of an oscillating aerofoil, whereas Digital Image Correlation (DIC) has been successfully used to monitor the deformation of propeller blades in-flight [22] and rotor blades [23].

Despite the perceived relative abundance of experimental test data regarding propeller and rotor aeroelastics, experimental efforts prior to 1970 typically made use of blades with vague geometric dimensions and non-homogeneous structural properties. In contrast, later investigations are well defined, however, when all investigations are consid-

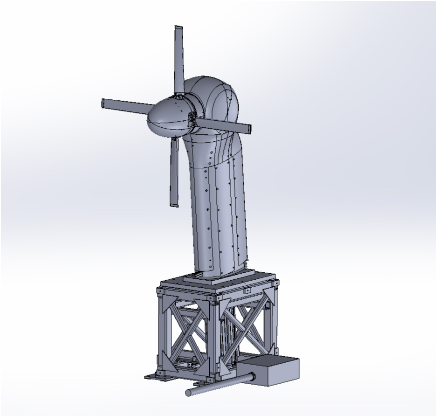

Figure 1: ARA Rotor Rig - Propeller Mode.

ered together there is no clear testing strategy or database that can be formed due to changing blade shapes, materials, rotational speeds, advance ratios and fluid properties. Considering all of the aforementioned factors, the existing available experimental data is no longer suitable to validate modern numerical models.

The purpose of this paper is to detail the development of the UK National Rotor Rig (UKNRR) in the framework of the EPSRC funded MENtOR project. This rig has been modified at the University of Glasgow from an already existing rig developed at the Aircraft Research Association (ARA) to allow for the investigation of Mach-scaled propellers in close to stall conditions, making use of state-of-the-art instrumentation. The development, features and capabilities of the UKNRR will be addressed whilst also providing practical insight to considerations of integrating a complex rig into an existing wind tunnel. Finally, sample results of the MENtOR tiltrotor blade set at a stalled condition will be presented and discussed.

2. DEVELOPMENT OF UKNRR

2.1. Initial design and scope of UKNRR

The ARA rotor rig[24] was originally designed to allow testing of both helicopter and tiltrotor configurations in three facilities, the ARA Transonic Wind Tunnel, the University of Glasgow's deHavilland tunnel and the University of Southampton's RJ Mitchell tunnel. A rendering of the rotor rig in propeller mode is shown in Figure 1. The rig was powered by an electric motor which could provide up to 77 kW of power and allowed a maximum rotational frequency of 3000 RPM.

In helicopter configuration, the rig allowed a shaft tilt angle ranging between +/-20°, while in tiltrotor configuration, a shaft tilt angle between -20° and +90° could be achieved. A maximum tilt rate of 10°/s was possible.

The four bladed hub was fully articulated and incorporated a RSB which measured the hub loads in six degrees of freedom. Two sets of baseline instrumented blades were part of the rig, one representing a typical helicopter blade design and the other being more representative of tiltrotor blades. All of the blades were instrumented with strain gauges intended to allow the flapping, torsion and lead-lag bending mode shapes to be measured. The diameter of the helicopter rotor was 1.8 m, with a maximum rotational frequency of 2300 RPM, whilst the diameter of the tiltrotor was 1.4 m, with a maximum rotational frequency of 3000 RPM. The maximum allowable hub loads, used for the design of the RSB and including both the static and dynamic components of the loading are shown in Table 1.

A digital Datatel telemetry system was mounted in the hub allowing for the transmission of data signals from instrumentation on the rotating frame of the rig to the stationary frame, as well as providing the power for the transducers. Off-body measurement systems such as Constant Temperature Anenmometry (CTA) and Laser Doppler Anemometry (LDA) to probe the flow and Digital Image Correlation (DIC) to monitor blade deflections also formed part of the rotor rig.

Despite its promising capabilities, the rig was never fully finalised as the funding of the project ended while also facing vibration issues arising from the gearbox that allowed the tilting movement.

2.2. Relocation of UKNRR to University of Glasgow and rig adaptation

The UKNRR was then relocated to the University of Glasgow in the framework of the EPSRC funded MENtOR project. In order to make the rig useful for the scope of the project, i.e. testing of propellers in close to stall configurations, a series of modifications were undertaken. The main modification consisted of the removal of the gearbox that allowed the tilting motion and the repositioning of the motor on top of the wing structure, so that it could directly drive the propeller. This adaptation allowed for the bypassing of the vibratory issues that the rig had up to that moment and restored the available motor

Table 1: ARA Rotor Rig - Maximum allowable loads

Thrust	3400	N
Torque	350	Nm
Side Forces	550	N
Pitching moment/Rolling moment	250	Nm

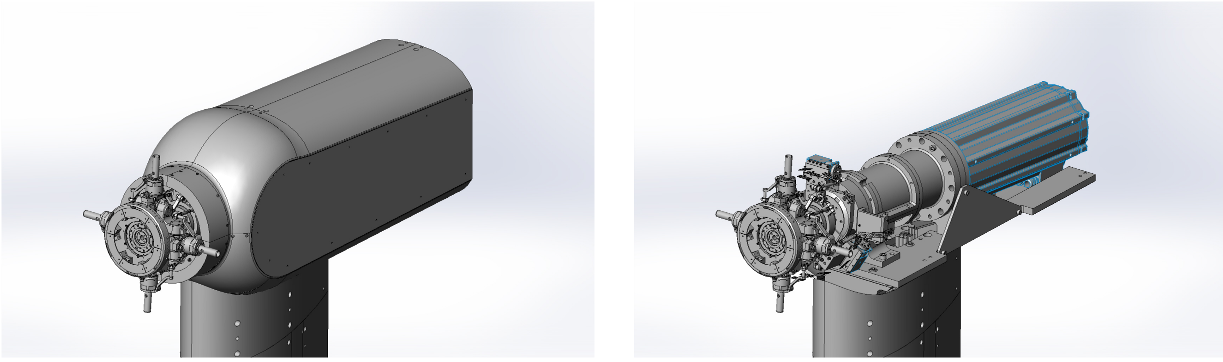

(a) New design with fairing.

(b) New design, fairing removed.

Figure 2: New direct-drive design.

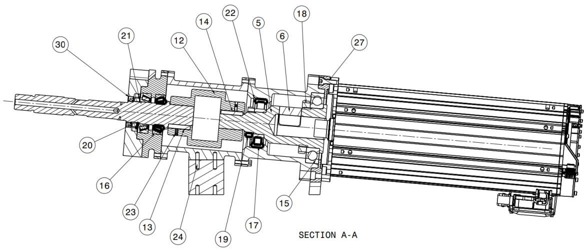

Figure 3: Schematic of the internal structure of the drive-train.

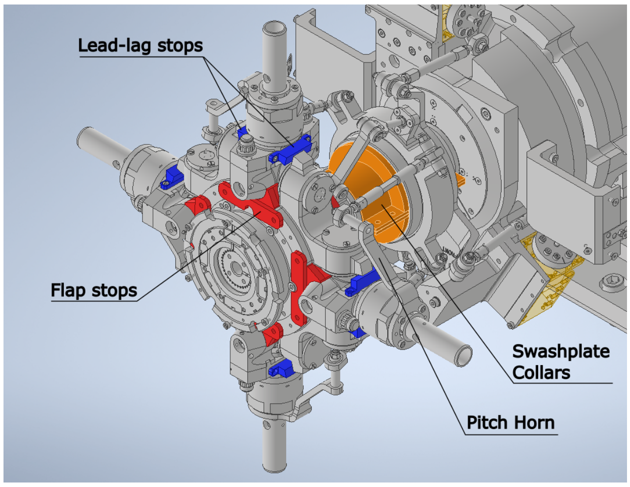

Figure 4: Rotor hub with flap, lead-lag stops and swashplate collars installed.

power to the original 125 kW, previously capped at 77kW by the gearbox. A render of the new design (with and without fairing, to appreciate the internal structure) is shown in Figure 2. Figure 3 shows a section of the internal structure of the drivetrain, to better highlight the connections between the different components. The motor is attached to the main frame through a flange (#27 on Figure 3) and one triangular plate on either side that can be seen in Figure 2(b). The motor shaft is then attached to an intermediate shaft (#5) which is free to rotate with respect to the main frame, thanks to two bearings (# 15 and #17). This intermediate shaft is then connected to the main output shaft through an Arcoflex TYPE314 flexible coupling (#12) in order to allow a small misalignment between the motor shaft and the output shaft.

Further modifications to the rig included the introduction of flap and lead-lag stops on the rotor hub to restrict the blade to a zero flapping and lead-lag angle to test and better simulate the behaviour of a propeller as presented in Figure 4. Swashplate collars, also represented in Figure 4, were designed, 3D printed and installed for a range of collective pitch angles to set both cyclic pitch angles to zero.

Considering the high pitch angles needed to test the rig in stall conditions, custom pitch adaptors were designed to be installed between the pitch horns and the pitch shaft so that the range of available pitch angle could be increased from $[-5°, 25°]$ to $[-5°, 40°]$. A summary of the updated rig operational limits after all these modifications is reported in Table 2. A photograph of the rig in the test section of the deHavilland wind tunnel, ready for testing with spinner and fairing on, can be found in Figure 5.

Table 2: Rotor Rig - Maximum allowable loads and operating conditions after modifications.

Thrust	3400	N
Torque	350	Nm
Side Forces	550	N
Pitching/Rolling moment	250	Nm
Max. Available power	125	kW
Max. Rotational Speed	3000	RPM
Pitch angle range	[-5, 40]	°

Figure 5: The UKNRR installed in the deHavilland tunnel.

2.3. Integration of UKNRR into deHavilland Wind Tunnel

A schematic of the rotor rig installed inside the test section (2.74m width x 2.1m height x 5m length) of the University of Glasgow deHavilland wind tunnel is presented in Figure 6. Due to the presence of the turntable, the rig was installed so that the propeller plane would lie upstream of the centre of the test section, approximately 1 m downstream from the end of the contraction. The rig sits on top of a steel framework which is bolted to the ground and connected to the turntable behind. An aluminium wing section provides support to the motor, that spins the rotor through a direct drivetrain. The centre line of the motor-drivetrain-shaft-hub assembly is positioned in the centre of the wind tunnel working section , and the rig is free from any contact with the tunnel floor. Due to the relatively slender nature of the upper part of the rotor rig and the presence of very heavy components at the top of the supporting structure, a modal test campaign was carried out by Tatar et al.[25] to assess the modal characteristics and the resonances that the rig might have to cross during the spin-up and spin-down procedures.

3. FEATURES AND CAPABILITIES OF UKNRR

3.1. MENtOR Blades

A set of 1.4m diameter tiltrotor blades was included in the original rotor rig. However, it was later shown through CFD simulations that the original set was not suitable for the envisaged application in the MENtOR project, as they would stall at excessively high collective pitch angles and the torque and power required in close to stall conditions exceeded the maximum limits allowable on the rig. A re-design of the blades was undertaken at the University of Glasgow[26] to overcome these problems.

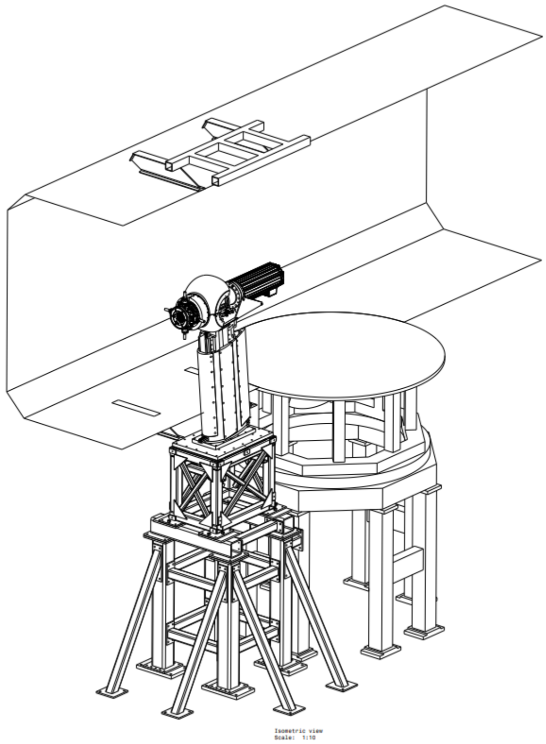

Figure 6: Schematic of the modified UKNRR installed in the deHavilland WT.

Several modifications were carried out in terms of twist, thickness and chord distribution, however the most important change was the reduction of the rotor diameter from 1.4 m to 1.25 m.

Each blade is instrumented with fully bridged shear and axial strain gauges, totalling seven bridges per blade. Strain gauges were installed on the internal surface of the blade composite skin to allow for review of bridge time histories and spectral content of the blade structural response. Strain gauge bridges have been placed at various locations along the spanwise and chordwise directions, shown on Figure 7, to measure flap bending (FB), lead-lag bending (LB) and torsional twist (T). Bridge locations were determined during the design of the blade which made use of coupled CFD and CSD simulations[26]. In particular, bending bridges are composed of four axial strain gauges oriented in the spanwise direction, of which two gauges are co-located on the upper blade surface and two on the lower, at the same spanwise location. This full-bridge arrangement compensates for centrifugal loading and thermal deformation.

3.2. Rotating Shaft Balance

A custom design six component RSB, capable of obtaining all three forces (F_x, F_y, F_z) and three mo-

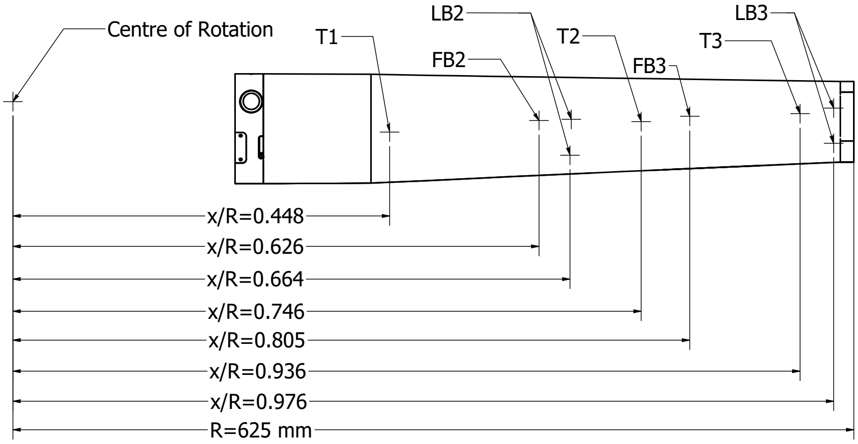

Figure 7: Location of flap-bending (FB), lead-lag (LB) and torsional (T) strain gauge bridges on the instrumented blade.

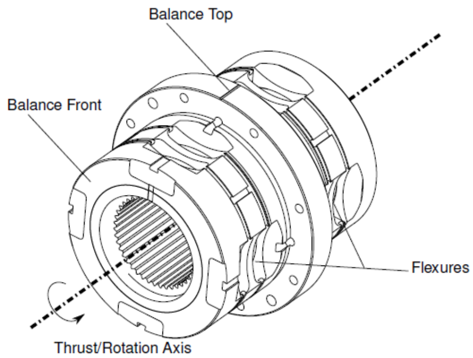

(a) RSB design.

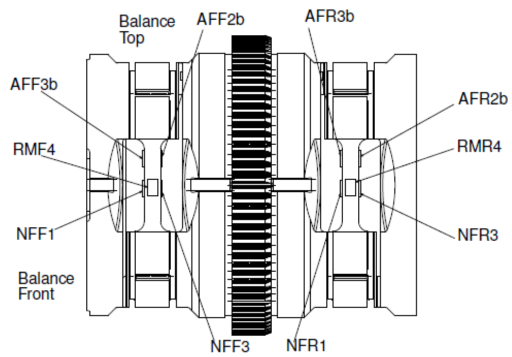

(b) Strain gauge locations - Port view.

Figure 8: Sketches of UK national rotor rig custom built RSB.

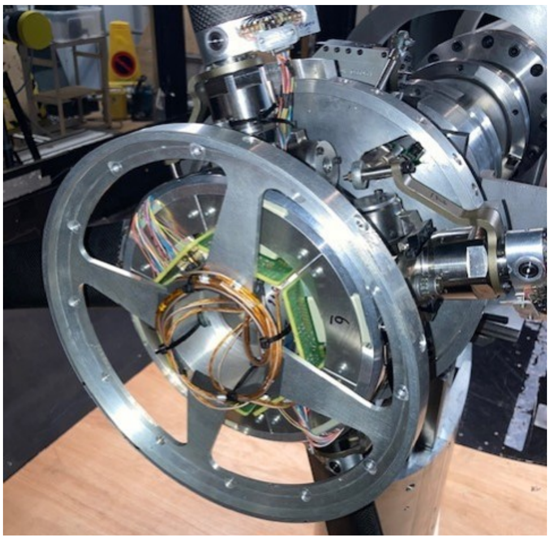

(a) Telemetry installed on the rotor hub.

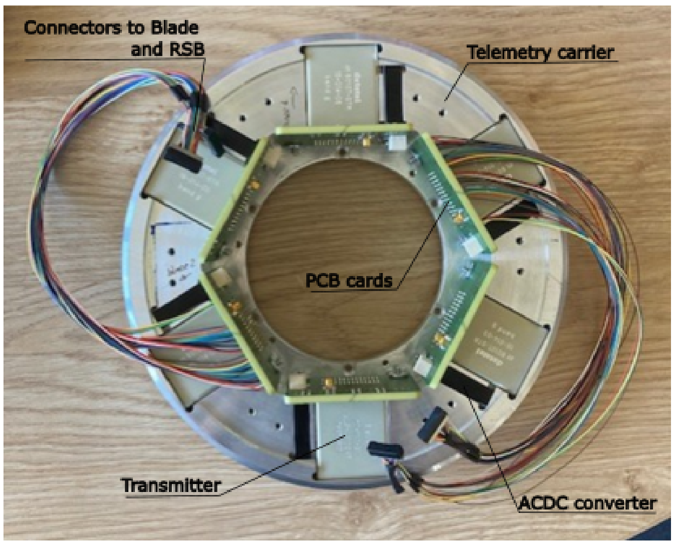

(b) Telemetry carrier, transmitters and connections.

Figure 9: Details of the Datatel telemetry installation on the UKNRR.

ments (M_x, M_y, M_z) acting on the propeller, was bespoke manufactured for the UKNRR by ARA and is shown in Figure 8(a). The maximum allowable loads for the RSB are shown in Table 1.

The RSB is instrumented with 32 strain gauges, positioned on flexures at various positions around the balance, displayed in Figure 8(b), that are arranged to form 8 full bridge configurations. To resolve the in-plane moments, two additional bridges are required with respect to the 6 axes, to measure the difference in loading between the fore and the aft part of the balance, hence why eight bridge voltages are recorded. The RSB is currently in the final stage of integration onto the rig and is planned to be used in the next test campaign.

3.3. Telemetry System

A Datatel digital telemetry system was mounted on the hub, as depicted in Figure 9(a). The telemetry allows for the transmission of data signals from instrumentation on the rotating frame of the rig to the stationary frame, as well as providing the power for the transducers. The telemetry system comprises 60 channels (six transmitters of 10 channels each) and is currently configured to transmit data from the RSB measuring the hub loads and strain gauges in one of the blades. The telemetry carrier hosting the six transmitters, PCB cards and connectors is shown in Figure 9(b). Power to the transducers and signal back to the receiver are transmitted from the rotating part of the rig to the stationary part by means of an inductive coil endowed with antenna positioned at the hub mount.

4. WIND TUNNEL INTERFACE

4.1. Measurement of Velocity in the Working Section

The integration of the UKNRR in the deHavilland wind tunnel presented a challenge in how to accurately and reliably determine the wind tunnel speed at which the propeller was subjected to. As reported in section 2.3, the presence of the turntable forced the rig to be installed upstream of where models are usually located in the test section, in a position where the propeller plane was aligned with the main Pitot-static probe. This prevented the sole use of the Pitot-static probe to accurately measure the freestream velocity, due to the influence of the propeller slipstream on the probe. Therefore, to provide a reliable reference pressure measurement to be used to set the wind tunnel speed, a differential pressure transducer was used to measure the pressure difference across two rings of pressure tappings at the entrance and exit of the contraction section, as this measurement was deemed to be less affected by the influence of the propeller.

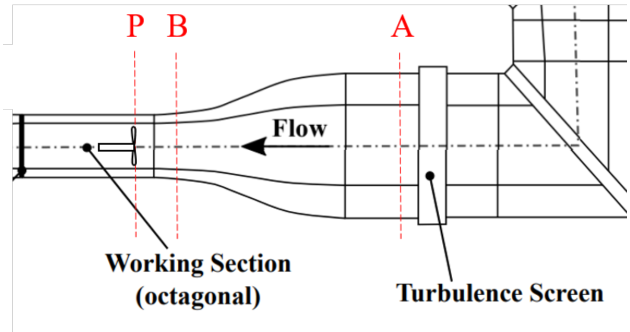

Figure 10: Schematic of the wind tunnel test section and contraction, with the position of the propeller plane and Pitot-static probe (P), and the locations of the pressure tap rings at the entrance (A) and exit (B) of the contraction.

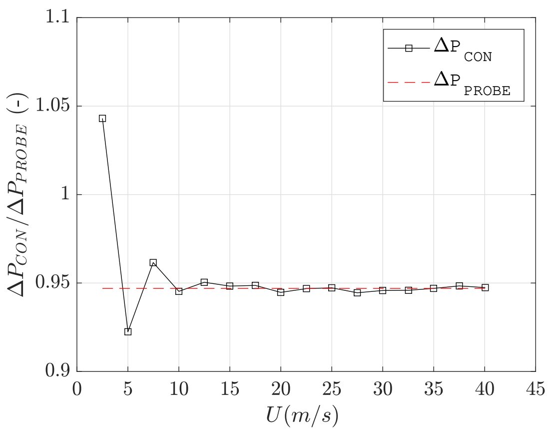

Figure 11: Calibration of the deHavilland wind tunnel using pressure measurements from the wind tunnel Pitot-static probe and contraction ring.

Figure 10 clearly shows the location of the Pitot-static probe (P), in addition to the locations of the pressure tapping rings at the entrance (A) and exit (B) of WT contraction.

To ensure the wind tunnel velocity measurements obtained by measuring the pressure difference across the contraction were meaningful, a wind tunnel calibration was performed with the UKNRR situated within the working section with its blades removed. The calibration was performed by measuring the pressure difference across the contraction ($\Delta P_{CON} = P_A - P_B$) and the dynamic pressure of the Pitot-static probe (ΔP_{PROBE}) within the working section for a series of wind tunnel fan settings. Measurements were obtained between

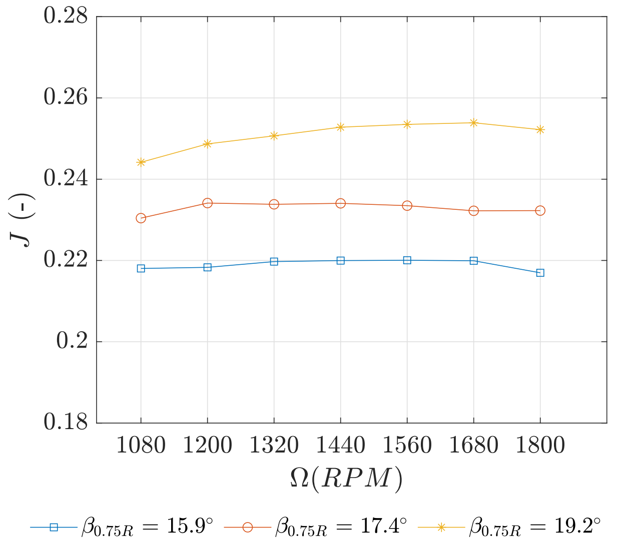

Figure 12: Recirculation induced advance ratio as a function of the propeller Ω.

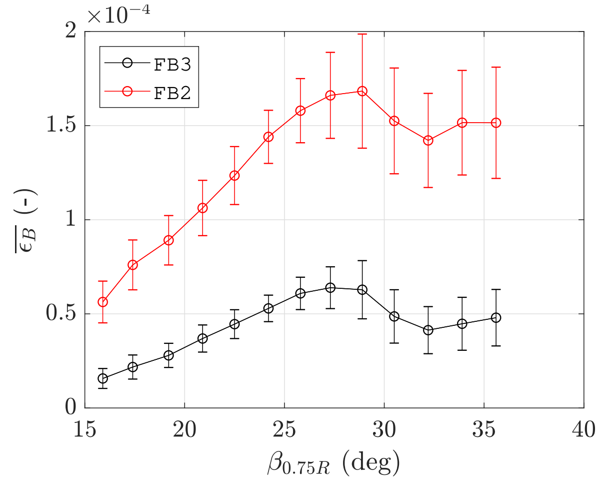

Figure 13: Compensated strain for bridges FB2 and FB3 at 1080 RPM and J=0.5 as a function of the blade pitch angle. Standard deviation of the measurements has been added as error bar.

$U_\infty = 0 - 40$ m/s at a resolution of $\Delta U_\infty = 2.5$ m/s. Results are presented in Figure 11 in terms of the ratio $\kappa = \Delta P_{CON}/\Delta P_{PROBE}$. It is shown that the average ratio across the range of free-stream velocities is $\kappa = 0.947$, which is within a sensible range of the theoretical value of $\kappa_{Ideal} = 24/25 = 0.96$ that can be obtained when considering a contraction ratio of 5:1. Values of κ at $U_\infty \leq 7.5$ m/s display some level of drift from the average ratios due to the dynamic pressure being relatively small and being more affected by measurement noise. Once the calibration was completed, the reference dynamic pressure used to set the wind tunnel speed was set to be $q = \Delta P_{CON}/\kappa$.

4.2. Recirculation of Propeller Induced Velocity

A side effect of testing the propeller within a closed-loop wind tunnel, such as the deHavilland, was that the air entrained by the propeller would recirculate around the wind tunnel loop, in such way that the propeller would act as a second wind tunnel fan. The magnitude of the recirculation was dependant on the propeller pitch setting, and dictated the minimum advance ratio at which the propeller could be tested.

Figure 12 presents the measured advance ratio when the propeller was spun at varying RPM, for several pitch settings, with the wind tunnel fan not being operated. At low $\beta_{0.75R}$, the induced advance ratio is constant with respect to Ω, implying that the propeller works at constant thrust coefficient throughout the range of RPM investigated. As the blade pitch is increased, the J curves move upwards as the thrust coefficient grows. The curve for $\beta_{0.75R} = 19.2°$ starts to bend down in the low RPM range, a behaviour that can be considered a precursor of stall, as less thrust is generated.

5. SAMPLE RESULTS

Finally, sample results from a recent test campaign are presented in this section to highlight the rig capabilities. For further details about the test campaign and commentary of the results, please refer to Croke at al.[27].

Figure 13 shows the compensated strain for bridges FB2 and FB3 at 1080 RPM and J=0.5, as a function of the blade pitch angle. The compensated strain $\overline{\epsilon_B}$ is introduced to compare cases recorded at different rotational frequencies and densities, and is defined as:

$$\overline{\epsilon_B} = \epsilon_B \frac{\overline{\rho}}{\rho} \left(\frac{\overline{\Omega}}{\Omega}\right)^2 \tag{1}$$

where $\overline{\rho}$ is the reference density (i.e. 1.225 kg/m^3), $\overline{\Omega}$ is the reference rotational speed, i.e. 1800 RPM and ϵ_B is the non compensated bridge reading.

Flap bending bridges, FB2 and FB3, are located at spanwise locations$x/R = 0.62$ and $x/R = 0.8$ respectively. Flap stops to restrict the flapping motion of the blade were installed on the rotor hub. Therefore, the higher readings of strain at FB2 when compared to those of FB3 can be explained by the fact that the blade was operating like a cantilever beam. The onset of stall can be clearly identified at $\beta_{0.75R} = 22.5°$ as there is a noticeable deviation

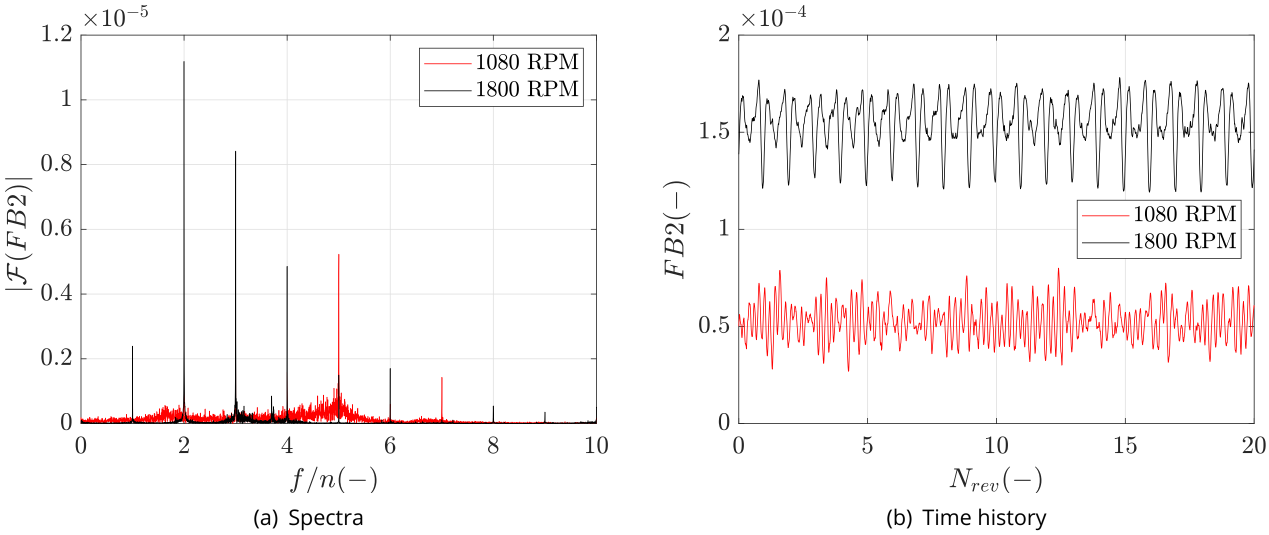

Figure 14: Amplitude of the Fourier transform (as a function of the non dimensional frequency f/n) and time history (as a function of the number of revolutions) of the uncompensated strain measurements for FB2 at $\beta_{0.75R} = 30.5°$ and J=0.5.

from the linear behaviour seen until this point. This can also be supported by the analysis of the bridge measurement standard deviation (represented as an error bar in Figure 13), which clearly indicates a sudden growth in magnitude for $\beta_{0.75R} \geq 22.5°$ due to the presence of more unsteadiness in the flow. Considering that the bending bridges measure the strain caused by the overall load acting from their position until the end of the blade (i.e. $0.8 \leq x/R \leq 1$ for FB3 and $0.62 \leq x/R \leq 1$ for FB2), and after the stall onset both FB2 and FB3 readings drop by roughly the same amount, this suggests that most of the stall develops towards the blade tip.

To further indicate the presence of stall, analysis of the strain spectral content and its time history was undertaken and presented in Figure 14 for $\beta_{0.75R} = 30.5^o$ at J=0.5. It is clear from Figure 14(a) that at 1080 RPM a significant non-harmonic content across a broadband of frequencies is observed when the propeller harmonics at multiple integers of its rotational frequency are also displayed. 1800 RPM is represented by the propeller harmonics only and does not appear to show a large broadband content which is a result of the propeller not operating in a stalled condition at 1800 RPM. Spectral analysis is expected to provide insight into whether the propeller blade is stalled, as for a stalled case there will be a large non-harmonic content as the signal energy is distributed amongst a large range of frequencies. In contrast, a propeller in a non-stalled condition should display a content that clearly shows the fundamental frequency and its harmonics. This is further validated by the time histories of Figure 14(b), where the 1080 RPM signal shows no repeatable pattern nor consistency in the amplitude of the oscillation, whereas the 1800 RPM signal shows a repetitive pattern of consistent amplitude.

6. CONCLUDING REMARKS

The development of a novel propeller test rig for testing in close to stall conditions has been described in the present paper. The rig makes use of a tiltrotor blade set instrumented with strain gauges to monitor flap bending, lead-lag bending and torsion, together with a rotating shaft balance that measures the load acting on the propeller. Data is transmitted from the rotating to the stationary frame of the rig by means of a telemetry system.

A calibration of the wind tunnel was undertaken to obtain a reliable reference wind tunnel velocity that was not affected by the presence of the propeller.

Sample strain gauge data was shown to validate the capability of the test rig to correctly identify stall and assess the unsteadiness of the blade structural response, by looking at the strain time histories and their spectra.

ACKNOWLEDGMENTS

This research is funded by the U.K. Research Council (EPSRC) Methods and Experiments for Rotorcraft (MENtOR), Grant EP/S013814/1.

REFERENCES

[1] Katzmayr, R., "Deflection of propeller blades while running," Techincal Memorandum 145, National Advisory Committee for Aeronautics, Washington, D.C, USA, 1922.

[2] Seewald, F., "Flutter in propeller blades," Techincal Memorandum 642, National Advisory Committee for Aeronautics, Washington, D.C, USA, 1931.

[3] Theodorsen, T., "Propeller vibrations and the effect of the centrifugal force," Techincal Note 516, National Advisory Committee for Aeronautics, Langley Field, VA, USA, 1935.

[4] Sterne, L., "Spinning tests on fluttering propellers," Reports & Memoranda 2022, Aeronautical Research Council, London, England, UK, 1945.

[5] Baker, J. E. and Paulnock, R. S., "Experimental investigation of flutter of a propeller with clark y section operating at zero forward velocity at positive and negative blade-angle settings," Techincal Note 1966, National Advisory Committee for Aeronautics, Langley Air Force Base, VA, USA, 1949.

[6] Gray, W. and Allis, A., "The torsional deflection of several propellers under operating conditions," Research Memorandum L51A19, National Advisory Committee for Aeronautics, Langley Field, VA, USA, 1951.

[7] O'Bryan, T. C., "Flight measurements of the vibratory bending and torsional stresses on a modified supersonic propeller for forward mach numbers up to 0.95," Techincal Note 4342, National Advisory Committee for Aeronautics, Langley Field, VA, USA, 1958.

[8] O'Bryan, T. C., "Flight measurements of the vibratory stresses on a propeller designed for an advance ratio of 4.0 and a mach Number of 0.82," Techincal Note 4410, National Advisory Committee for Aeronautics, Langley Field, VA, USA, 1958.

[9] O'Bryan, T. C., "Flight measurements of the vibratory and torsional stresses on a supersonic-type propeller for forward mach numbers up to 0.95," Research Memorandum L56D20a, National Advisory Committee for Aeronautics, Langley Field, VA, USA, 1956.

[10] Hubbard, H. H., Burgess, M. F., and Slyvester, M. A., "Flutter of thin propeller blades, including effects of mach number, structural damping, and vibatory-stress measurements near the flutter boundaries," Techincal Note 3707, National Advisory Committee for Aeronautics, Langley Field, VA, USA, 1956.

[11] Whitlow Jr, J. and Sievers, G., "Fuel savings potential of the NASA Advanced Turboprop Program," Aviation Fuel Conservation Symposium,Washington, D.C, USA, 10-11 Sep 1984.

[12] Kaza, K., Mehmed, O., Williams, M., and Moss, L., "Analytical and experimental investigation of mistuning in propfan flutter," 28th Structures, Structural Dynamics and Materials Conference, Monterey, CA, USA, 06-08 Apr 1987.

[13] Smith, A. F. and Brooks, B. M., "Dynamic response and stability of a composite prop-fan model," Contractor Report 179528, Hamilton Standard Divsion United Technologies Corporation, Windsor Locks, CT, USA, 1986.

[14] Smith, A. F. and Brooks, B. M., "Dynamic response of two composite prop-fan models on a nacelle/wing/fuselage half model," Contractor Report 179589, Hamilton Standard Divsion United Technologies Corporation, Windsor Locks, CT, USA, 1986.

[15] Mehmed, O. and Kaza, K., "Experimental classical flutter results of a composite advanced turboprop model," Techincal Memorandum 88792, National Aeronautics and Space Administration, Lewis Research Center, OH, USA, 1986.

[16] Mehmed, O., "Propfan model wind tunnel aeroelastic research results," *NASA, Lewis Research Center, Lewis Structures Technology*, Vol. 1: Structural Dynamics, 1988.

[17] Burton, P., "Straingauge test report on a spin test carried out on a Type(c) R.305/3-82-F/6 propeller on the spinning tower at the R.A.E Farnborough, Hunts," Test report 093.1.592, DOWTY ROTOL Limited, Gloucester, England, UK, 1979.

[18] Podboy, G. and Krupar, M., "Laser velocimeter measurements of the flow field generated by a forward-swept propfan during flutter," 23rd Fluid Dynamics, Plasmadynamics, and Lasers Conference, Orlando, FL, USA, 06-09 Jul 1993.

[19] Poirel, D., Goyaniuk, L., and Benaissa, A., "Frequency lock-in in pitch–heave stall flutter," *Journal of Fluids and Structures*, Vol. 79, 2018, pp. 14–25.

[20] Ringenberg, H. C. and Farnsworth, J. A., "Transient growth and decay of aeroelastic stall flutter," AIAA Scitech 2022 Forum, San Diego, CA, USA, 3-7 Jan 2022.

[21] Bhat, S. S. and Govardhan, R. N., "Stall flutter of NACA 0012 airfoil at low Reynolds numbers," *Journal of Fluids and Structures*, Vol. 41, 2013, pp. 166–174.

[22] Boden, F., Stasicki, B., Szypuła, M., Ružička, P., Tvrdik, Z., and Ludwikowski, K., "In-flight

measurements of propeller blade deformation on a VUT100 cobra aeroplane using a co-rotating camera system," *Measurement Science and Technology*, Vol. 27, 2016, pp. 074013.

[23] Sicard, J. and Sirohi, J., "Measurement of the deformation of an extremely flexible rotor blade using digital image correlation," *Measurement Science and Technology*, Vol. 24, (6), 2013, pp. 065203.

[24] Morales, R., Turner, M., Platts, J., Pugh, D., and McCallum, A., "Control design of a tilting mechanism for the UK National Rotor Test Rig Facility," 43rd European Rotorcraft Forum, Milam, Italy, 12-15 Sep 2017.

[25] Tatar, A., Wu, J., Zagaglia, D., Titurus, B., Rezgui, D., Green, R., and Barakos, G., "Modal characterisation of a rotor/propeller rig for tip-mach scaled wind tunnel testing," 47th European Rotorcraft Forum, Virtual Meeting, 6-9 Sep 2021.

[26] Woodgate, M. A., Fitzgibbon, T. A., and Barakos, G., "The Use of Computational Fluid Dynamics in the Investigation of Stall Onset on Tilt-Rotor Blades," 47th European Rotorcraft Forum, Virtual Meeting, 6-9 Sep 2021.

[27] Croke, A. D., Zagaglia, D., Woodgate, M. A., Green, R. B., and Barakos, G. N., "Experimental investigation into the onset of stall flutter on tiltrotor blades," 49th European Rotorcraft Forum, Bückeburg, Germany, 05-07 Sep 2023.